Modeling coating flaws with non-linear polarization curves for long pipelines

D.P. Riemer[1] & M.E. Orazem[2]
[1] *OLI Systems, Inc., USA.*
[2] *Department of Chemical Engineering, University of Florida, USA.*

Abstract

External corrosion is commonly mitigated by coating the structure with a high resistance film and by employing cathodic protection (CP) to protect regions that are inadequately coated or where the coating has degraded. Defects in the coating are termed holidays, and such holidays can expose bare steel. The objective of this paper is to explore the state-of-the-art in computer models for cathodic protection. The emphasis is placed here on mitigation of corrosion of underground pipelines, but the concepts, models, and techniques described are sufficiently general to be applied to mitigation of corrosion of any structure.

1 Introduction

Since the beginning of the 20th century, petroleum products and natural gas have been transported over long distances by buried steel pipelines. Over 1.3 million miles of buried steel main-line pipe are used to transport natural gas within the United States [1]. An additional 170,000 miles of pipeline are used to transport crude oil and refined petroleum products [2].

The limited availability of right-of-way corridors requires that new pipelines be located next to existing pipelines. Placement of pipelines in close proximity introduces the potential for interference between systems providing cathodic protection to the respective pipelines. In addition, the modern use of coatings, introduced to lower the current requirement for cathodic protection of pipelines, introduces as well the potential for localized failure of pipes at discrete coating defects. The prediction of the performance of cathodic protection systems under these conditions

WIT Transactions on State of the Art in Science and Engineering, Vol 7, © 2005 WIT Press
www.witpress.com, ISSN 1755-8336 (on-line)
doi:10.2495/1-85312-889-9/09

requires a mathematical model that can account for current and potential distributions in both angular and axial directions.

The objective of this work is to describe a mathematical model that has been developed for cathodic protection of an arbitrary number of pipelines linked to an arbitrary number of cathodic protection systems. The Boundary Element Method was used in the model formulation. In order to achieve the desired calculation accuracy and speed, the development required significant refinement to algorithms available in the literature.

2 Mathematical development

The model for cathodic protection of pipelines must account for the flow of current in the soil, in the pipes, and in the circuitry. Until recently, most models of cathodic protection of pipelines assumed that the potential of the pipe steel was uniform. The assumption of a uniform steel potential enabled solution for current and potential distributions without consideration of the passage of current through the pipe. Long pipes, however, exhibit a non-negligible potential difference along the steel [3–5].

In the context of the present work, there exist two separate domains for the flow of current. The first is the soil (or outer) domain, bounded by the surfaces of the pipes and anodes, the interface between the soil and air, and, if present, the interface between the soil and any buried insulating layers. The second (inner) domain comprises the metallic wall of the pipe, the volume of the anode, and connecting wires and resistors for the return path of the protective current. The two domains are linked by the electrochemical reactions described in section 2.3.

2.1 Soil (or outer) domain

The soil domain comprises the material in which the pipes and anodes are buried. From the perspective of the pipe, this domain can be considered to be an outer domain. This designation contrasts the soil domain from the domain which includes the interior volume of pipeline steel.

In principle, the treatment of concentrations and potential within the soil requires solution of a coupled set of equations, including conservation of each individual solute species [6], $i.e.$

$$\frac{\partial c_i}{\partial t} = -(\nabla \cdot \boldsymbol{N}_i) + R_i \tag{1}$$

and an expression of electroneutrality

$$\sum_i z_i c_i = 0 \tag{2}$$

where c_i is the concentration of species i, R_i is the rate of generation of species i due to homogeneous reactions, and $\boldsymbol{N}_i$ is the net flux vector for species i. In a dilute

electrolytic solution, the flux $\boldsymbol{N}_i$ includes contributions from convection, diffusion, and migration as

$$\boldsymbol{N}_i = \boldsymbol{v}c - D_i \left[\nabla c_i - \frac{z_i c_i F}{RT} \nabla \Phi \right] \tag{3}$$

where $\boldsymbol{v}$ is the fluid velocity, D_i is the diffusion coefficient for species i, z_i is the charge associated with species i, F is Faraday's constant, and Φ is the potential.

Under the assumption of a steady-state and a uniform concentration of ionic species, the current density, expressed in terms of contributions from the motion of each ionic species, can be given in terms of potential by Ohm's law. Thus,

$$\boldsymbol{i} = F \sum_i z_i \boldsymbol{N}_i = -\kappa \nabla \Phi \tag{4}$$

where the conductivity κ, expressed in terms of contributions from individual species as

$$\kappa = F^2 \sum_i z_i^2 u_i c_i \tag{5}$$

has a uniform value because the concentration is uniform. The assumption that concentrations are uniform yields

$$\nabla^2 \Phi = 0. \tag{6}$$

Thus, potential is governed by Laplace's equation.

Equation (6) is commonly used without explanation in cathodic protection models. The development presented above can be used to emphasize some important points.

- The assumption that concentrations are uniform means that concentration gradients associated with reactions on the pipe and anode surface are assumed to occur within a thin layer adjacent to the pipe and anode surfaces. The concentration gradients within this narrow layer can be incorporated into the boundary condition which describes the electrochemical reactions.
- While changes in soil resistivity can be treated within Boundary Element models by creating coupled soil domains, the variation of potential across the boundaries between domains must include the contribution of a diffusion potential associated with concentration gradients.

The resistivity of the soil domain was assumed to be uniform in the present model.

2.2 Pipe metal (or inner) domain

The potential drop within the pipeline steel can be very significant when the current level is large and the pipelines are long. The Ohmic resistance of a ANSI Standard 18-inch (0.457m) diameter steel pipe with a wall thickness of 0.375 inches (0.95cm) is 7.2×10^{-3} Ω/km. The potential drop along a 100km length of this pipe would be 720mV for passage of a relatively modest 1A of CP current. The assumption that the potential drop in the pipe steel can be neglected, made, for example, by Esteban

et al [7] for their treatment of coating holidays in a short length of pipe, cannot be made for longer stretches of pipeline networks.

The flow of current through the pipe steel, anodes, and connecting wires is strictly governed by the Laplace's equation

$$\nabla \cdot (\kappa \nabla V) = 0 \tag{7}$$

where V is the departure of the potential of the metal from a uniform value and κ is the material conductivity. The conductivity of the pipe-metal domain κ is not necessarily uniform. For example, the copper wires connecting the pipe to the anode have a different conductivity than does pipeline steel or the anode, or groundbed material. A simplified version of eqn (7)

$$\Delta V = IR = I\rho\frac{L}{A} \tag{8}$$

can be used to account for the potential drop across connecting wires, where R is the resistance of the wire, ρ is the electrical resistivity, L is the length, and A is the cross-sectional area of wire.

2.3 Domain coupling through boundary conditions

The inner and outer domains described in sections 2.1 and 2.2, respectively, are linked by boundary conditions which relate the current density on metal surfaces to values of local potential. The type of surface governs the specific form of the relationship required. Bare steel, coated steel, galvanic anodes, and impressed current anodes are considered in the following sections.

2.3.1 Bare steel

While the surface of modern pipelines are generally covered by a protective coating, bare metal can be exposed by coating defects caused by mechanical damage or long-term degradation mechanisms. For steel in soil, the electrochemical reactions include corrosion, oxygen reduction, and, at sufficiently cathodic potentials, hydrogen evolution. One common form of the boundary condition, adapted for steady-state soil systems by Yan *et al* [8] and Kennelly *et al* [9], takes the form

$$i = 10^{(V-\Phi-E_{Fe})/\beta_{Fe}} - \left(\frac{1}{i_{\lim,O_2}} - 10^{(V-\Phi-E_{O_2})/\beta_{O_2}}\right)^{-1} - 10^{-(V-\Phi-E_{H_2})/\beta_{H_2}} \tag{9}$$

where V is the potential of the steel, obtained from solution of the inner domain, and Φ is the potential of the soil adjacent to the steel, obtained from solution of the outer domain. The term β_{Fe} represents the Tafel slope for the corrosion reaction, and E_{Fe} represents the equilibrium potential for the corrosion reaction. Similar terms are used for the oxygen reduction and hydrogen evolution reactions.

The mass transfer of oxygen is taken into account by including the mass transfer limited current density for oxygen reduction $i_{\mathrm{lim},\mathrm{O}_2}$.

The influence of calcareous and corrosion-product films on the bare surface can be taken into account by adjusting the kinetic parameter values. Nisançiöglu [10–12] showed how the parameters of polarization curves can be adjusted in CP models to account for the influence of polarization history in transient models. Carson and Orazem suggested a refined regression approach to obtain time-dependent polarization parameters [13]. Polarization curves can be obtained for specific chemical compositions through predictive mathematical models such as that given by Anderko *et al* [14, 15]. The principle is that the current contributions for individual reactions are summed to yield a relationship between local current density, the potential of the steel, and the potential of the soil adjacent to the steel.

2.3.2 Coated steel

Application of coatings to steel before burial reduces the amount of current required to provide cathodic protection. These coatings are usually polymeric but can sometimes be cement-based products.

Cathodic protection must nevertheless be used for coated pipes. Isolated faults in the coating (termed holidays) can form galvanic couples with the coated portion, thereby accelerating the corrosion of the bare steel exposed by the holiday. The pipeline will experience failure due to corrosion in a far shorter time than would be experienced if the pipe were left bare [3].

The coated portion of steel is often treated as an insulator or as a simple high-resistance electronic conductor. To explore the role of galvanic coupling, however, the electrochemical reactions on the coated steel must be treated explicitly. It has been reported that a small current will pass through some coatings after they have absorbed sufficient amounts of water [16–20]. Corfias *et al* have shown that the pore structure expands as the coating absorbs water [17]. They have also shown that the coating conductivity increases significantly with immersion time.

Two possible modes for transport through a coating are illustrated schematically in fig.1. Figure 1(a) represents a uniform barrier in which ionic species enter a polymeric phase. The electrochemical reaction is assumed to take place at the metal-coating interface, driven by the potential difference $V - \Phi_{\mathrm{in}}$. Figure 1(b) represents a metal covered by an insulating coating perforated by pores through which ionic

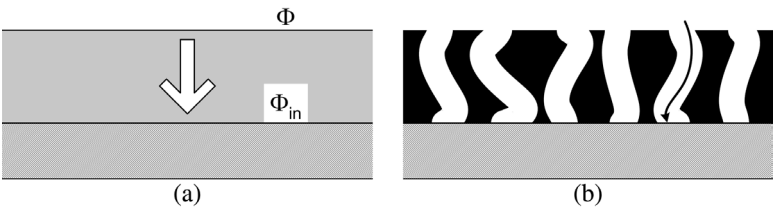

Figure 1: Schematic representation of two models for coating behavior: a) coating allowing uniformly distributed transport of species, and b) coating with discrete pores through which transport can take place.

species may move. The effective resistivity of the coating then depends on the number of pores per unit area. Again, the electrochemical reaction is assumed to take place at the metal-coating interface and is driven by the potential difference $V - \Phi_{\text{in}}$. The view of a coated steel represented in fig. 1 is supported by results reported by NOVA Gas [21] and CC Technologies [19, 22, 23], which showed that coatings on steel pipe formed a diffusion barrier when placed in aqueous environments, that the coating absorbs water, and that it is possible to polarize slightly the steel under a disbonded coating.

The modification of eqn (9) by Riemer and Orazem [24, 25] can address either mode of transport illustrated in fig. 1. The potential drop through the film or coating can be expressed as [7]

$$i = \frac{\Phi - \Phi_{\text{in}}}{\rho\delta} \tag{10}$$

where Φ is the potential in the electrolyte next to the coating, Φ_{in} is the potential at the underside of the coating just above the steel, ρ is the effective resistivity of the coating and δ is the thickness of the coating. The current density can also be written in terms of the electrochemical reactions as

$$i = \frac{A_{\text{pore}}}{A}\left[10^{(V-\Phi_{in}-E_{Fe})/\beta_{Fe}} - \left(\frac{1}{(1-\alpha_{blk})\,i_{lim,O_2}} - 10^{(V-\Phi_{in}-E_{O_2})/\beta_{O_2}}\right)^{-1} - 10^{-\left(V-\Phi_{in}-E_{H_2}\right)/\beta_{H_2}}\right] \tag{11}$$

where A_{pore}/A is the effective surface area available for reactions, and α_{blk} is the reduction to the transport of oxygen through the barrier. It is also assumed that the coating has absorbed enough water that the hydrogen evolution reaction is not mass-transfer limited. Equations (10) and (11) are solved simultaneously by a Newton–Ralphson method to get values for the current density and Φ_{in}.

By eliminating the current density in eqns (10) and (11), a particularly useful equation is obtained as

$$\frac{A\,(\Phi - \Phi_{\text{in}})}{A_{\text{pore}}\rho_{\text{film}}\delta_{\text{film}}} = 10^{(V-\Phi_{\text{in}}-E_{\text{Fe}})/\beta_{\text{Fe}}} - \left(\frac{1}{(1-\alpha_{\text{blk}})\,i_{\text{lim},\text{O}_2}} - 10^{(V-\Phi_{\text{in}}-E_{\text{O}_2})/\beta_{\text{O}_2}}\right)^{-1} - 10^{-\left(V-\Phi_{\text{in}}-E_{\text{H}_2}\right)/\beta_{\text{H}_2}} \tag{12}$$

which links V, Φ, and Φ_{in}. Equation (12) can be solved by a Newton–Ralphson method to get Φ_{in} for given values of V and Φ. The current density can subsequently be calculated from eqn (10).

The corrosion potential of the coated steel can be calculated from eqn (11) under the assumption that no current flows through the coating. If $(1 - \alpha_{\text{blk}})$ is smaller

than the pore ratio, then the metal will be more active than bare steel. If they are the same, then the coated pipe and bare steel will have the same corrosion potential. If $(1 - \alpha_{\mathrm{blk}})$ is larger than the pore ratio, the metal under the coating will be more noble than the bare steel and will contribute to a galvanic couple that, in the absence of CP, will enhance the corrosion rate at the holiday.

2.3.3 Galvanic anodes

The treatment of electrochemical processes at galvanic or impressed-current anodes is similar to that used in section 2.3.1 for bare steel. A galvanic anode is selected to be anodic to the metal to be protected. Zinc and magnesium are used to protect carbon steel in soil environments, and aluminum and magnesium are used in sea water. The aluminum–steel couple does not provide a sufficient driving force to be effective in soil where the resistivity is typically much higher than that of sea water.

The electrochemical reactions at the galvanic anode typically consist of oxygen reduction, assumed to take place at the mass-transfer-limited rate, and corrosion. The resulting expression is given as

$$i = i_{\mathrm{O}_2} \left(10^{(V - \Phi - E_{\mathrm{corr}})/\beta_{\mathrm{anode}}} - 1 \right) \tag{13}$$

where i_{O_2} is the mass-transfer-limited current density for oxygen reduction, E_{corr} is the free corrosion (equilibrium) potential of the anode, and β is the Tafel slope for the anode corrosion reaction. The assumption that oxygen reduction is mass-transfer-controlled is justified at the potentials typically seen for galvanic anodes. Hydrogen evolution was ignored for galvanic anodes because it only makes a small contribution to the net current at operating potentials. Some typical values reported in the literature for the model parameters used in eqn (13) are given in table 1. The value for the mass-transfer-limited current density must be obtained for specific soil conditions.

2.3.4 Impressed-current anodes

Impressed-current systems consist of a dimensionally stable (non-corroding) anode connected to the positive terminal of a direct-current (DC) rectifier. The negative terminal of the rectifier is connected to the pipe. The rectifier can then be used to push the potential of the anode to any desired potential that is more negative than that

Table 1: Parameters for common galvanic anodes [4].

Anode Type	E_{eql} (mV CSE)	β (mV/decade)	i_{O_2} $(\mu\mathrm{A/cm}^2)$
Al	-1.0	60	1.0
Zn	-1.1	60	1.0
Mg (Standard)	-1.5	60	1.0
Mg (High Potential)	-1.75	60	1.0

Table 2: Parameters for the oxygen and chlorine evolution reactions [26].

Reaction	Equilibrium Potential (E)	Tafel Slope (β)
O_2 evolution	-172mV (CSE)	100mV/decade
Cl_2 evolution	50mV (CSE)	100mV/decade

of the pipe. Because the driving potential for impressed-current anodes is provided by an outside current source, the current densities obtainable on impressed-current systems are usually an order of magnitude larger than can be obtained with galvanic anodes. Impressed-current systems can therefore protect a much longer section of pipe and can be used to greater effect in highly resistive soils.

The anodic reaction at an impressed-current anode is typically water oxidation (evolution of oxygen)

$$2H_2O \rightarrow O_2 + 4H^+ + 4e^- \tag{14}$$

and, at more anodic potentials, chloride oxidation (evolution of chlorine)

$$2Cl^- \rightarrow Cl_2 + 2e^-. \tag{15}$$

The cathodic reaction would be the reduction of oxygen, just as was seen in eqn (13) for galvanic anodes. Thus, the polarization model for an impressed-current anode resembles that for galvanic anodes with the exception that an additional term is added to account for the potential setting of the rectifier, $i.e.$

$$i = i_{O_2}\left(10^{(V-\Phi-\triangle V_{\rm rect}-E_{O_2})/\beta_{O_2}} - 1\right) \tag{16}$$

where $\triangle V_{\rm rect}$ is the potential added by the rectifier, V is the voltage of the anode, Φ is the voltage just outside the surface of the anode, E_{O_2} is the equilibrium potential for the oxygen evolution reaction, and β_{O_2} is the tafel slope for the oxygen evolution reaction.

If chloride ions are present, eqn (16) must be modified to account for the contribution of the chlorine evolution reaction (15). Reaction (15) takes place in environments such as salt marshes and estuaries which can contain significant amounts of salt.

Kinetic parameters for reactions (14) and (15) are given in table 2. Again, the mass-transfer-limited current density for oxygen reduction i_{O_2} must be determined experimentally for a specific location.

3 Numerical development

Laplace's equation has been solved for many boundary conditions and domains [27]. Analytic and semi-analytic formulations can be used for specific geometries. For example, Moulton first applied the Schwartz-Christoffel transformation to calculate analytically the conduction of current through a two-dimensional rectangular geometry with arbitrarily placed electrodes [28]. Bowman supplies details for analytic

solutions using the Schwartz-Christoffel transformation [29]. Orazem and Newman provide a semi-analytical implementation of the Schwartz-Christoffel transformation for the more complicated structure of a slotted electrode [30]. Orazem used the technique for a compact tension fracture specimen [31] which was later further refined [32]. Diem *et al* take the semi-analytical technique a step further by allowing for insulating surfaces to form an arbitrary angle with the electrode [33].

Unfortunately, such analytic and semi-analytic approaches are not sufficiently general to allow all the possible configurations of pipes within a domain, the detailed treatment of potential variation within the pipes, and the polarization behavior of the metal surfaces. Thus, numerical techniques are required. Of the available techniques, the boundary element method is particularly attractive because it can provide accurate calculations for arbitrary geometry. The method only solves the governing equation on the boundaries, which is ideal for corrosion problems where all the activity takes place at the boundaries. Brebbia first applied the boundary element method for potential problems governed by Laplace's equation [34]. Aoki [35] and Telles [36] reported the first practical utilization of the boundary element method with simple nonlinear boundary conditions. Zamani and Chuang demonstrated optimization of cathodic current through adjustment of anode location [37].

The pipe steel domain is solved using the finite element method. Brichau first demonstrated the technique of coupling a finite element solution for pipe steel to a boundary element solution for the soil [38]. He also demonstrated stray current effects from electric railroad interference utilizing the same solution formulation [39]. However, Brichau's method was limited in that it assumed that the potential and current distributions on the pipes and anodes were axisymmetric allowing only axial variations. Aoki presented a technique similar to Brichau's that included optimization of anode locations and several soil conductivity changes for the case of a single pipe with no angular variations in potential and current distributions [40, 41].

Since it is desired to have a solution for the current and potential distributions both around the circumference and along the length of the pipe, Brichau's method must be modified. These modifications are described in the following sections. The elements of the BEM and FEM techniques which are well established in the literature are summarized here for completeness.

3.1 Outer domain: boundary element method

The boundary element method can be derived from the same technique used to obtain the classical finite element method. One starts by writing a variational or weighted residual of the governing differential equation. If the PDE takes the form

$$\nabla^2 u - f = 0 \tag{17}$$

where f is a forcing term that is a function of position only, then one would write

the weighted residual as

$$\int_{\Omega} w\left(\nabla^2 u - f\right) d\Omega = 0, \forall w \tag{18}$$

where Ω is the domain and w is any weighting function. In the case of Laplace's equation, $f = 0$ and $u = \Phi$; thus

$$\int_{\Omega} w \nabla^2 \Phi d\Omega = 0, \forall w. \tag{19}$$

This equation holds for all weighting functions w. Equation (19) is integrated analytically by using the divergence theorem

$$\int_{\Omega} \nabla w \nabla \Phi d\Omega - \int_{\Gamma} w\left(\vec{n} \cdot \nabla \Phi\right) d\Gamma = 0, \forall w \tag{20}$$

with Γ being the boundary of the domain. Equation (20) is the classical weak form of the finite element method for Laplace's equation. At this stage, the boundary element method development departs from the finite element method by using a second application of the divergence theorem. The highest order derivative is thereby moved to the weighting function, $i.e.$

$$\int_{\Omega} \Phi \nabla^2 w d\Omega - \int_{\Gamma} w\left(\vec{n} \cdot \nabla \Phi\right) d\Gamma + \int_{\Gamma} \Phi\left(\vec{n} \cdot \nabla w\right) d\Gamma = 0, \forall w. \tag{21}$$

At this point the weighting function needs to be specified to show why the second application of the divergence theorem was done. If one observes that the solution to the equation

$$\nabla^2 G_{i,j} + \delta_i = 0 \tag{22}$$

is the Greens function for Laplace's equation, one can simplify eqn (21) by picking the weighting function to be the Green's function [42]. The first integral in eqn (21) becomes

$$\int_{\Omega} \Phi\left(-\delta_i\right) d\Omega = -\Phi_i. \tag{23}$$

Substitution of eqn (23) into eqn (21) yields a simpler equation valid within the domain

$$\Phi_i + \int_{\Gamma} \Phi\left(\vec{n} \cdot \nabla G_{i,j}\right) d\Gamma = \int_{\Gamma} G_{i,j}\left(\vec{n} \cdot \nabla \Phi\right) d\Gamma \tag{24}$$

where the highest order derivative has been removed and all the integrals are along the boundaries only. Equation (24) is still exact in so far as the Green's function is known and is valid for determining the values of the potential at any interior point in the domain given that the potential and current density distributions on the boundary are known. This implies that, for Laplace's equation, values of interior points are fully specified by integrals along the boundary only.

The last step in deriving the Boundary Element method is to take Φ_i to the boundary. A Cauchy principle value is introduced in the integral on the left side of

eqn (24). It is usually represented by a constant appearing in front of the first term in eqn (24)

$$c_i \Phi_i + \int_\Gamma \Phi \left(\vec{n} \cdot \nabla G_{i,j}\right) d\Gamma = \int_\Gamma G_{i,j} \left(\vec{n} \cdot \nabla \Phi\right) d\Gamma. \tag{25}$$

For a smooth surface at the point i, the constant c_i is equal to π [43].

3.1.1 Infinite domains

Everything done to this point has been done under the assumption that the boundary encloses the domain. In many situations, the domain lies outside the boundary. In order to get a solution for this situation, it is necessary to introduce a second boundary, $\bar{\Gamma}$, placed around the surface of interest and centered on the source point on that surface. Adding the enclosing boundary to eqn (25), one obtains

$$\begin{aligned} c_i \Phi_i + \int_\Gamma \Phi \left(\vec{n} \cdot \nabla G_{i,j}\right) d\Gamma + \int_{\bar{\Gamma}} \Phi \left(\vec{n} \cdot \nabla G_{i,j}\right) d\bar{\Gamma} \\ = \int_\Gamma G_{i,j} \left(\vec{n} \cdot \nabla \Phi\right) d\Gamma + \int_{\bar{\Gamma}} G_{i,j} \left(\vec{n} \cdot \nabla \Phi\right) d\bar{\Gamma}. \end{aligned} \tag{26}$$

If the radius of the new boundary is taken to infinity then the limit of the integrals over the external boundary, $\bar{\Gamma}$, go to infinity

$$\lim_{R \to \infty} \left(\int_{\bar{\Gamma}} \Phi \left(\vec{n} \cdot \nabla G_{i,j}\right) d\bar{\Gamma} - \int_{\bar{\Gamma}} G_{i,j} \left(\vec{n} \cdot \nabla \Phi\right) d\bar{\Gamma} \right) = H_{i,\infty}. \tag{27}$$

The value of eqn (27) can be found analytically

$$- \int_{\Gamma_\infty} \Phi \left(\vec{n} \cdot \nabla G_{i,j}\right) d\Gamma_\infty = H_{i,\infty} = 4\pi\Phi \tag{28}$$

where the minus sign indicates the direction of the normal vector. The second term in eqn (27) vanishes as the limit is taken. The value of integral in (28) can be more easily seen if it is transformed to spherical coordinates

$$\lim_{r \to \infty} \left(- \int_0^\pi \int_0^{2\pi} \frac{\Phi}{r^2} \left(r^2 \sin\phi\right) d\theta d\phi \right) = 4\pi\Phi \tag{29}$$

where r is also the normal vector since the surface is a sphere centered at a source point. Φ at infinity is often assumed to be zero; thus satisfying the zero radiation condition at infinity exactly.

3.1.2 Half spaces

A half space is simply an infinite domain split by a plane. The half space is the space lying on one side of the plane. If either the Dirichlet or Neumann condition vanishes at the plane, the Green's function presents an interesting opportunity to satisfy that condition exactly with a very small additional computation when evaluating the

kernels of the integrals. This is done by making use of the reflection properties of Green's functions [43–46]. In the case of buried pipelines, the Neumann condition vanishes at the plane boundary, $i.e.$ there is no current flowing out of the soil into the air, and none is flowing from the air into the soil.

If one starts with the boundary condition on the plane being zero normal current and places a source at x and its reflection about the plane at x' [46],

$$\sigma(x)(\vec{n}\cdot\nabla G(x,\xi)) + \sigma(x')(\vec{n}\cdot\nabla G(x',\xi)) = 0 \tag{30}$$

which implies that the two source intensities $\sigma(x)$, and $\sigma(x')$ are equal and have the same sign. The sign is the same because the outward normal vectors have opposite signs for the z component for the reflections. The final form of the Green's function is

$$G_{i,j} = \frac{1}{4\pi r(x_i, x_j)} + \frac{1}{4\pi r(x_i, x'_j)} \tag{31}$$

where x'_j is the reflected source point.

3.1.3 Layers

Layers are created using the same types of Green's function reflections as described above. The only restriction is that one of the two boundary conditions at the interface between the two layers must be equal to zero ($i.e.$ either $\Phi = 0$ or $\vec{n}\cdot\nabla\Phi = 0$) [46]. In the context of cathodic protection of buried pipelines, the only boundary condition that has physical meaning is a zero normal current condition since there is no easy way to have an arbitrary plane within the electrolyte that has a potential equal to zero. Including a plane with a zero Neumann (natural) condition implies that there is one region in which current may flow that is bounded by regions of zero conductivity whose boundaries are defined by the Green's function reflections. An example would be an underlying rock layer which has zero conductivity.

The resulting functions can be obtained by using equations of the form of eqn (30). The Green's function in three dimensions would then be of the form

$$G_{i,j} = \sum_{k}^{\text{Reflections}+1} \frac{1}{4\pi r(x_i, x_{j,k})} \tag{32}$$

where the index $k > 1$ refers to the reflection about some plane k. For $k = 1$, $x_{j,k}$ is the field point on the real object. If the soil surface is the only reflection used, the result is the same as eqn (31).

An example of a pipeline in a halfspace with an underlying rock layer is shown in fig. 2. Two reflections were used. The first accounts for the zero normal current at the air–soil interface which is represented by the pipe in the air. The second reflection accounts for the zero normal current at the rock soil interface and is represented by the lower pipe.

The influence of the nonconducting layer on the current delivered to a pipe is seen in fig. 3 for a sequence of calculations for which the distance r between the horizontal pipe and a non-conducting layer placed below the pipe was varied.

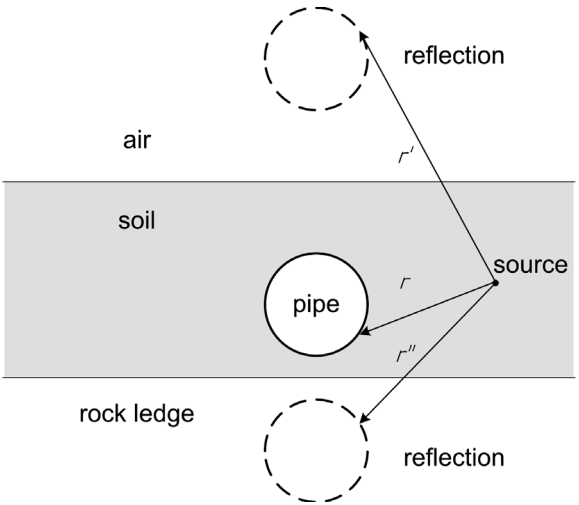

Figure 2: Reflections of Green's function to account for boundaries with zero normal current.

For these calculations, the anode was placed far from the pipe such that the current distribution around the circumference of the pipe was affected only by the screening of the insulating ledge. The current increased with the distance according to

$$\frac{I}{I_{r\to\infty}} = 1 - \frac{a}{\sqrt{r}} \tag{33}$$

where a is a fitted parameter that depends on the geometry and soil resistance and $I_{r\to\infty}$ is the value obtained from Dwight's formula [3, 47] which does not account for the presence of a nonconducting layer. The total current tended toward that predicted by Dwight's formula as the distance between the ledge and the pipe increased.

3.2 Inner domain: finite element method

The Finite Element Method was used for the domain consisting of the pipe-line steel, copper connection wires, and anode material. The Finite Element Method is ideal for completely bounded domains where the material properties may change from one location to another, $i.e.$ current flow from the pipe to the copper wire connecting the pipe to the anode. A significant advantage of the formulation was that the same discretization could be employed as was used for the Boundary Element Method solution of the outer domain.

The development of the finite element method for the pipe steel domain starts by writing a weighted residual for the strong form of Laplace's equation given in eqn (7)

$$\int_{\Omega} w\nabla\cdot\vec{\vec{\kappa}}\cdot\nabla V d\Omega = 0 \tag{34}$$

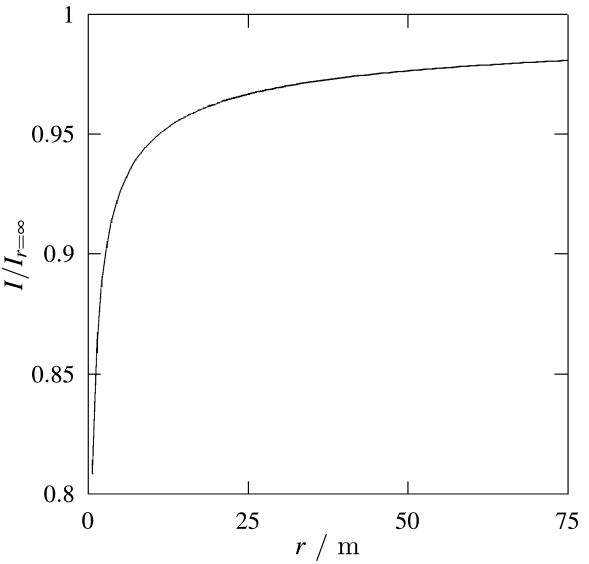

Figure 3: Total calculated current, normalized by the result from Dwight's formula for an infinite soil domain [3,47], as a function of the separation r between the pipe and an underlying (insulating) rock layer.

where w is any weighting function. For pipe steel, κ is just a constant times an identity matrix

$$\vec{\vec{\kappa}} = \kappa \begin{bmatrix} 1 & 0 & 0 \\ 0 & 1 & 0 \\ 0 & 0 & 1 \end{bmatrix} \tag{35}$$

with step changes in κ when the type of metal changes. After substituting the material properties into eqn (34) and integrating by parts using the divergence theorem, the following Weak Form is obtained

$$\int\int\int_{\Omega} \kappa \nabla w \cdot \nabla V \, dx \, dy \, dz = -\oiint w \kappa \, (\vec{n} \cdot \nabla V) \, ds \tag{36}$$

where $\vec{n}$ is the outward normal vector from the boundary of the domain. The domain is divided into elements using piecewise continuous polynomial isoparametric shape functions. The shape functions approximate the geometry and solution, V, over the elements. The discretized form of eqn (36) is

$$\sum_{j=1}^{n} \left[\int\int\int_{(e)} \kappa \nabla \phi_i^{(e)} \cdot \nabla \phi_j^{(e)} \, dx \, dy \, dz \right] V_j = -\oiint \kappa \phi_i^{(e)} \, (\vec{n} \cdot \nabla V)_i^{(e)} \, ds \tag{37}$$

where κ is the scalar component of the property tensor, ϕ_i is a shape function and the sum goes from 1 to the total of all the shape functions of all the elements.

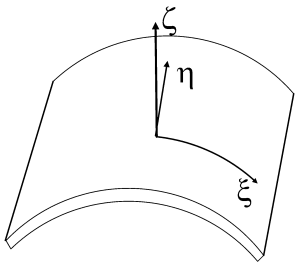

Figure 4: Diagram of the shell element used to calculate the potential drop within the pipe steel. The element is assumed to have no variation in the ζ direction. The curvilinear coordinate system is displayed on top of the element.

3.2.1 Pipe shell elements

A special type of thin shell elements is introduced here and shown in fig. 4. These elements are specifically designed for potential problems on shells where the absolute value of the material property (κ in eqn (37)) is large.

The elements are defined in orthonormal curvilinear coordinates, ξ, η, and ζ where ξ and η define the outside surface of the pipe and ζ is the outwardly directed normal vector. ζ is obtained through the cross product $\xi \times \eta$.

Variations of the potential in the ζ direction were assumed to be negligible because the scale of the problem is many orders of magnitude greater in the ξ and η directions. Variations of the potential parallel to the surface were allowed to vary in a piece-wise continuous way using bi-quadratic shape functions for the elements. These functions were obtained through the product of two Lagrange interpolating polynomials of the same order, one in ξ and one in η. The result is a family of elements with square parent elements which include the four-node linear, the nine-node quadratic, and the 16 node cubic elements.

3.2.2 Applying elements to the FEM

The integral (37) must be transformed to the curvilinear coordinate system of the parent elements. A differential volume, $dx\,dy\,dz$ can be transformed to the curvilinear system by the determinate of the Jacobian of the coordinate transformation

$$dx\,dy\,dz = |\mathbf{J}|\,d\xi\,d\eta\,d\zeta \tag{38}$$

where $\mathbf{J}$ is the Jacobian.

The Jacobian is composed of the partial derivatives of the coordinates x, y and z with respect to each of the curvilinear coordinates

$$\mathbf{J} = \begin{bmatrix} \frac{\partial x}{\partial \xi} & \frac{\partial y}{\partial \xi} & \frac{\partial z}{\partial \xi} \\ \frac{\partial x}{\partial \eta} & \frac{\partial y}{\partial \eta} & \frac{\partial z}{\partial \eta} \\ \frac{\partial x}{\partial \zeta} & \frac{\partial y}{\partial \zeta} & \frac{\partial z}{\partial \zeta} \end{bmatrix}. \tag{39}$$

Integral (37) is transformed to the curvilinear coordinate system to yield

$$\sum_i \left[\int\int\int_{\Omega^{(e)}} \sum_k \frac{\partial \phi_i}{\partial x_k} \kappa \cdot \frac{\partial \phi_j}{\partial x_k} |\mathbf{J}| d\xi \, d\eta \, d\zeta \right] = - \iint_{\Gamma_{(e)}} w\kappa (\vec{n} \cdot \nabla V) \, ds \quad (40)$$

where x_k is one of the cartesian coordinates, $|\mathbf{J}|$ is the determinate of the Jacobian, s is the surface of the element $\vec{n}$ is the outward normal vector from the surface, and $\Omega^{(e)}$ is the domain of the parent element. The limits of integration in the parent element are from -1 to $+1$ for all three of the coordinates. For the special shell elements used for pipes, the integral is only performed numerically over the surface $d\xi \, d\eta$ which is then scaled by the physical thickness of the shell h, the result of the integral over ζ. This requires the Jacobian to be modified to a surface Jacobian which, in this case, is simply the square root of the magnitude of the Jacobian. Rewriting eqn (40), the two-dimensional integral over the surfaces of the pipes is obtained as

$$\sum_i \left[h \int\int_{\Omega^{(e)}} \sum_k \frac{\partial \phi_i}{\partial x_k} \kappa \cdot \frac{\partial \phi_j}{\partial x_k} \sqrt{|\mathbf{J}|} d\xi \, d\eta \right] = - \iint_{\Gamma_{(e)}} w\kappa (\vec{n} \cdot \nabla V) \, ds \quad (41)$$

with the thickness of the steel, h, a parameter. The normal vector has the same direction as the one from the boundary element method.

Partial derivatives in eqn (41) with respect to cartesian coordinates need to be expressed in terms of the curvilinear coordinates. Using the chain rule, but starting from the derivatives in cartesian coordinates, one writes

$$\left\{ \begin{array}{l} \frac{\partial \phi}{\partial x}\frac{\partial x}{\partial \xi} + \frac{\partial \phi}{\partial y}\frac{\partial y}{\partial \xi} + \frac{\partial \phi}{\partial z}\frac{\partial z}{\partial \xi} \\ \frac{\partial \phi}{\partial x}\frac{\partial x}{\partial \eta} + \frac{\partial \phi}{\partial y}\frac{\partial y}{\partial \eta} + \frac{\partial \phi}{\partial z}\frac{\partial z}{\partial \eta} \\ \frac{\partial \phi}{\partial x}\frac{\partial x}{\partial \zeta} + \frac{\partial \phi}{\partial y}\frac{\partial y}{\partial \zeta} + \frac{\partial \phi}{\partial z}\frac{\partial z}{\partial \zeta} \end{array} \right\} = \left\{ \begin{array}{l} \frac{\partial \phi}{\partial \xi} \\ \frac{\partial \phi}{\partial \eta} \\ \frac{\partial \phi}{\partial \zeta} \end{array} \right\} \quad (42)$$

or, in terms of the Jacobian

$$\mathbf{J} \left\{ \begin{array}{l} \frac{\partial \phi}{\partial x} \\ \frac{\partial \phi}{\partial y} \\ \frac{\partial \phi}{\partial z} \end{array} \right\} = \left\{ \begin{array}{l} \frac{\partial \phi}{\partial \xi} \\ \frac{\partial \phi}{\partial \eta} \\ \frac{\partial \phi}{\partial \zeta} \end{array} \right\}. \quad (43)$$

Since ϕ is a function of ξ, η, and ζ, the partial derivatives of ϕ with respect to the cartesian coordinates can be found by inverting the Jacobian.

$$\left\{ \begin{array}{l} \frac{\partial \phi}{\partial x} \\ \frac{\partial \phi}{\partial y} \\ \frac{\partial \phi}{\partial z} \end{array} \right\} = \mathbf{J}^{-1} \left\{ \begin{array}{l} \frac{\partial \phi}{\partial \xi} \\ \frac{\partial \phi}{\partial \eta} \\ \frac{\partial \phi}{\partial \zeta} \end{array} \right\}. \quad (44)$$

If $\mathbf{J}^{-1}_{i,j}$ is the element from the ith row and the jth column of the inverse of the Jacobian, then the partial derivatives defined in eqn (44) can be expanded to yield

$$\begin{aligned}
\frac{\partial \phi_i}{\partial x} &= (J^{-1})_{11}\frac{\partial \phi_i}{\partial \xi} + (J^{-1})_{12}\frac{\partial \phi_i}{\partial \eta} + (J^{-1})_{13}\frac{\partial \phi_i}{\partial \zeta} \\
\frac{\partial \phi_i}{\partial y} &= (J^{-1})_{21}\frac{\partial \phi_i}{\partial \xi} + (J^{-1})_{22}\frac{\partial \phi_i}{\partial \eta} + (J^{-1})_{23}\frac{\partial \phi_i}{\partial \zeta} \\
\frac{\partial \phi_i}{\partial z} &= (J^{-1})_{31}\frac{\partial \phi_i}{\partial \xi} + (J^{-1})_{32}\frac{\partial \phi_i}{\partial \eta} + (J^{-1})_{33}\frac{\partial \phi_i}{\partial \zeta}.
\end{aligned} \tag{45}$$

The assumption that the thickness of the shell is small with respect to the radius and length of the shell means that there is negligible variation in the potential in the ζ direction. Therefore, all terms in eqn (45) that involve partial derivatives with respect to ζ can be assumed to be equal to zero. All of the terms in eqn (41) can be evaluated numerically. Since the shape functions for the geometry and solution vary quadratically in the ξ and η directions, a nine-point Gauss rule (3×3) applied in both directions will give an exact (to machine precision) result.

3.2.3 Bonds and resistors

Bonds and resistors are used to provide paths for flow of electrical current between pipes or between pipes and anodes. Bonds were implemented as a linear 1D element between the connection node on one pipe or anode to the connection node on the second pipe or anode. This formulation requires introduction of no additional nodes. The material property is set by accounting for the real length and gauge of the wire that ties the pipes together. If a resistor is specified within the wire, it is added to the total resistance of the bond. An illustration of a bond is given in fig. 5. The lines connecting the pipes to each other and to the anode are bonds. The cylinder on the line connecting the two pipes represents a resistor that is sometimes added in series with the bond to adjust the current load applied to the pipelines. They are modeled as 1D finite elements that connect to the bond connection points. The value of the resistor is set to zero if a resistor is not used in the calculation.

A one-dimensional version of Laplace's equation is used for the 1D elements. The development for the linear 1D element follows that presented in section 3.2. The result of the integration over the bond is the total conductance of the bond or

$$K_e = \begin{bmatrix} \frac{1}{R} & \frac{-1}{R} \\ \frac{-1}{R} & \frac{1}{R} \end{bmatrix} \tag{46}$$

where R is the total resistance of the bond.

3.3 Coupling BEM to FEM

The finite-element model for the inner domain is coupled to the boundary-element for the outer domain at the interface between the two domains. Ohm's Law holds within each domain as stated in section 2.1. Therefore, at any arbitrary surface that forms a boundary between two domains it can be shown that the flux on either side

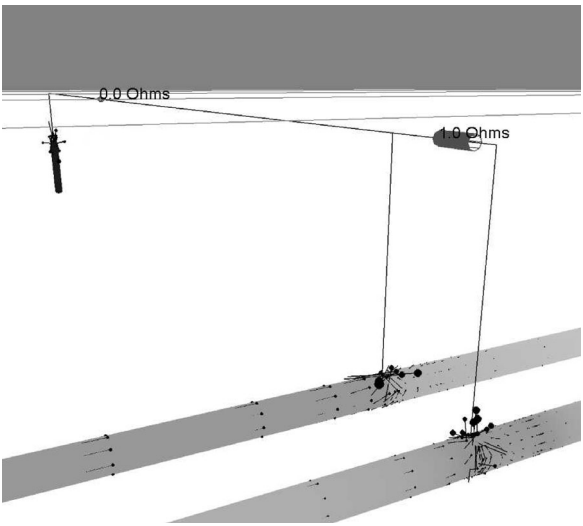

Figure 5: A representation of two horizontal pipes connected to each other and to a vertical anode or ground bed. The lines connecting the pipes to each other and to the anode are bonds. The cylinder on the line connecting the two pipes represents a resistor. They are modeled as 1D finite elements that connect to the bond connection points.

of the boundary is related by the material property,

$$\kappa_1 \vec{n} \cdot \nabla \Phi_1 = \kappa_2 \vec{n} \cdot \nabla \Phi_2 \tag{47}$$

which is a balance on charge at the pipe/soil interface, where κ is the material property. For potential problems, κ is the conductivity of the material in Mho/m. Using the variables for potential in the pipe, V, and potential in the soil, Φ, the interface condition is written as

$$(\vec{n} \cdot \nabla V) = \frac{\kappa_{\text{soil}}}{\kappa_{\text{steel}}} (\vec{n} \cdot \nabla \Phi) \tag{48}$$

where the quantity $\vec{n} \cdot \nabla V$ is used in the finite element load integral in eqn (41). Equation (48) can be inserted into eqn (41) to obtain

$$\sum_i \left[h \int\int_{\Omega^{(e)}} \sum_k \frac{\partial \phi_i}{\partial x_k} \kappa \cdot \frac{\partial \phi_j}{\partial x_k} \sqrt{|\mathbf{J}|} d\xi \, d\eta \right] = - \oint\!\!\!\!\!\!\int_{\Gamma_{(e)}} w \kappa_{\text{soil}} (\vec{n} \cdot \nabla \Phi) \, ds. \tag{49}$$

The right side of eqn (49) links the soil domain to the steel domain through the current density generated by the kinetics of the corrosion reaction at the steel surface given by eqns (9) and (12).

3.4 Discretization of the boundary elements

Equation (25) may now be applied to a surface that has its boundaries broken up into individual finite elements. The solution to the differential equation can be represented by approximate functions on each individual element. Example functions may be 0th order or constant value, 1st order or linear, *etc*. The simplest case is the constant element. The value of Φ is assumed to be constant across each element. Then one can write an equation of the form of (25) for each degree of freedom that makes up the surface and where the subscript i refers to the element number. The integrals are broken up into N sub-intervals corresponding to N elements that when summed together form the complete integral over the entire boundary

$$c_i\phi_i + \sum_j \int_{\Gamma_j} \Phi\,(\vec{n}\cdot\nabla G_{i,j})\,d\Gamma_j = \sum_j \int_{\Gamma_j} G_{i,j}\,(\vec{n}\cdot\nabla\Phi)\,d\Gamma_j. \tag{50}$$

When constant element are used, the unknown element potentials and normal current densities can be brought outside the integrals. Since a well-posed problem has one half of the boundary conditions specified, the result is N equations with N unknowns.

Since it is desired to be able to change the boundary condition type as well as value, the notation used here will denote the matrix resulting from the left hand integral as $\boldsymbol{H}$ and the right side as $\boldsymbol{G}$

$$\boldsymbol{H}\Phi = \boldsymbol{G}\,(\vec{n}\cdot\nabla\Phi) \tag{51}$$

where $\vec{n}\cdot\nabla\Phi$ is the normal current density divided by the conductivity at the boundary.

3.5 Self-equilibration

Cathodic protection systems are constrained by the requirement that charge is conserved. The boundary element formulation developed in section 2.1 requires modification to satisfy the constraint that charge is conserved. Instead of having a specified potential at infinity (most often set to zero) which serves as a source or sink for charge, an unknown value of potential at infinity is used such that no current enters or leaves through that boundary. To implement this condition, an extra equation is added to the system [36, 48]

$$\sum_i \int_{\Gamma_i} \kappa\hat{\vec{n}}\cdot\nabla\Phi d\Gamma_i = 0. \tag{52}$$

Equation (52) simply states that all currents entering the boundaries of the domain sum to zero, or, in other words, no current is lost to or gained from infinity. The left hand side is added as a new row at the bottom of the $\boldsymbol{G}$ matrix of eqn (51), while the matrix $\boldsymbol{H}$ in (51) receives a row of zeros. A column is added to the $\boldsymbol{H}$ matrix which

corresponds to the unknown potential at infinity. The values that are placed in this column come from eqn (28) and are all 4π or 1 depending on where the 4π from the Green's function is placed. This would make the $\boldsymbol{H}$ matrix singular because there is still a row of zeros in it. However, that would only be the case if Neumann type boundary conditions are specified everywhere. The Neumann problem results in an infinite number of solutions that differ by a constant. Therefore, at least one element in the system must have a Dirichlet boundary condition to make the $\boldsymbol{H}$ matrix nonsingular and result in a unique solution.

3.6 Multiple CP systems

Riemer and Orazem describe in detail the development needed to model interactions among CP systems [25]. To allow stray current between separate CP systems, additional rows can be added of the type introduced in eqn (52) [49]. For each separate CP system, one extra column in the $\boldsymbol{H}$ matrix is also added. The appearance of the matrices for 2 CP systems in the same domain will be

$$\boldsymbol{G} = \begin{bmatrix} G_{1,1} & G_{1,2} & G_{1,3} & G_{1,4} \\ G_{2,1} & G_{2,2} & G_{2,3} & G_{2,4} \\ 0 & 0 & A_3 & A_4 \\ A_1 & A_2 & 0 & 0 \end{bmatrix} \tag{53}$$

$$\boldsymbol{H} = \begin{bmatrix} H_{1,1} & H_{1,2} & 0 & 1 \\ H_{2,1} & H_{2,2} & 1 & 0 \\ 0 & 0 & 0 & 0 \\ 0 & 0 & 0 & 0 \end{bmatrix} \tag{54}$$

with the column matrix $\boldsymbol{u}$ given by

$$\boldsymbol{u} = \begin{bmatrix} u_1 \\ u_2 \\ u_{\infty,\mathrm{System2}} \\ u_{\infty,\mathrm{System1}} \end{bmatrix} \tag{55}$$

and the column matrix $\boldsymbol{q}$ defined in the usual way. When there are two or more CP systems within a domain, a Dirichlet condition on at least one element in each CP system must be specified to prevent the $\boldsymbol{H}$ matrix from being singular. The added equations and unknown potentials at infinity are sufficient to allow several CP systems to interact with each other while enforcing that the total current on each CP system sum to zero.

3.7 Nonlinear boundary conditions with attenuation in the pipe steel

The external load integral from the finite-element solution to the inner domain can be written for each node as a sum of contributions from each element that has that node in common

$$f_i = \sum_{\ell=1}^{nce} -\!\!\!\!\!\!\int\!\!\!\!\!\!\int_{\Gamma_{(e)}} w_{\ell,i}\kappa_{\text{soil}}\left(\vec{n}\cdot\nabla\Phi\right)ds \tag{56}$$

where f_i is the load for node i and nce is the number of contributing elements to the load at node i. This integral must be evaluated across all nodes on all surfaces of all structures in the model. Since the value of $\vec{n}\cdot\nabla\Phi$ is either a known or unknown boundary condition from the boundary element method, it must be factored out of the integral. Using the shape functions that describe the values of $\vec{n}\cdot\nabla\Phi$ across each element in terms of the nodal values $\vec{n}\cdot\nabla\Phi$ and the weights, one can rewrite eqn (56) as

$$f_i = \sum_{\ell=1}^{nce} -\!\!\!\!\!\!\int\!\!\!\!\!\!\int_{\Gamma_{(e)}} w_{\ell,i}\kappa_{\text{soil}} \sum_{k=1}^{nen} \phi_{\ell,k}(s)\left(\vec{n}\cdot\nabla\Phi\right)_{\ell,k} ds \tag{57}$$

where nen is the number of nodes in the element, $\left(\vec{n}\cdot\nabla\Phi\right)_k$ is the nodal value of the normal electric field within the element n, and $\phi(s)_k$ is the shape function whose value is one at node k. Using the property of integrals that an integral of a sum is the sum of integrals, eqn (57) can be rewritten as

$$f_i = \sum_{\ell=1}^{nce}\sum_{k=1}^{nen} -\!\!\!\!\!\!\int\!\!\!\!\!\!\int_{\Gamma_{(e)}} w_{\ell,i}\kappa_{\text{soil}}\phi_{\ell,k}(s)\left(\vec{n}\cdot\nabla\Phi\right)_{\ell,k} ds. \tag{58}$$

Equation (58) can then be written in matrix form as

$$f_i = \left[\ \ldots - \!\!\!\!\!\!\int\!\!\!\!\!\!\int_{\Gamma_{(e)}} w_{\ell,i}\kappa_{\text{soil}}\phi_{\ell,k}(s)ds\ \ldots\right] \begin{bmatrix} \left(\vec{n}\cdot\nabla\Phi\right)_{1,1} \\ \vdots \\ \left(\vec{n}\cdot\nabla\Phi\right)_{ne,nen} \end{bmatrix} \tag{59}$$

or

$$f_i = \hat{\boldsymbol{F}}_i\left[\vec{n}\cdot\nabla\Phi\right]. \tag{60}$$

These sub-matrices are then assembled with the right hand column matrix from eqn (51) to form the global finite element system

$$\boldsymbol{K}\left[V\right] = \hat{\boldsymbol{F}}\left[\vec{n}\cdot\nabla\Phi\right] \tag{61}$$

where $\hat{\boldsymbol{F}}$ is a matrix formed from the assembly of eqn (60) such that the column matrix corresponding to the Boundary Element Method is formed on the right hand side. $\hat{\boldsymbol{F}}$ is not symmetric.

4 Method for solution of systems of nonlinear equations

The set of variables that appear in the combined soil domain metal domain problem are potentials outside the surface of all pipes or tanks (Φ), unknown normal electric field on anodes ($\vec{n}\cdot\nabla\Phi$), and unknown potential difference ($V-\Phi$) for coated and bare protected structures. Introduction of the attenuation code from eqn (61) to the problem introduces n more equations and n more unknowns where n is the number of nodes used to describe the boundary mesh for the problem. The total number of algebraic equations to be solved is now $2n+k$, where k is the number of separate CP systems.

4.1 Global matrix

The coefficients obtained from the coupled methods are placed into a global matrix system and one instance of eqn (52) is added for self-equilibriation of each CP system

$$\begin{bmatrix} \boldsymbol{H}_{c,c} & \boldsymbol{H}_{a,c} & 0 & 0 & -4\pi \\ \boldsymbol{H}_{c,a} & \boldsymbol{H}_{a,a} & 0 & 0 & -4\pi \\ 0 & 0 & \boldsymbol{K}_c & 0 & 0 \\ 0 & 0 & 0 & \boldsymbol{K}_a & 0 \\ 0 & 0 & 0 & 0 & 0 \end{bmatrix} \begin{bmatrix} \Phi_c \\ \Phi_a \\ V_p \\ V_a \\ \Phi_\infty \end{bmatrix} = \begin{bmatrix} \boldsymbol{G}_{c,c} & \boldsymbol{G}_{a,c} \\ \boldsymbol{G}_{c,a} & \boldsymbol{G}_{a,a} \\ \hat{\boldsymbol{F}}_c & 0 \\ 0 & \hat{\boldsymbol{F}}_a \\ A_c & A_a \end{bmatrix} \begin{bmatrix} \vec{n}\cdot\nabla\Phi_c \\ \vec{n}\cdot\nabla\Phi_a \end{bmatrix} \tag{62}$$

where the subscripts a and c refer to anodes and cathodes (pipes), respectively, double subscripts are from the boundary element method and refer to where the source point and field point lie, respectively, and A is the area of each section.

The columns of eqn (62) are sorted such that all of the unknown variables are on the left hand side. For anodes, the unknown variable is the current density ($\vec{n}\cdot\nabla\Phi$), and for all other structures it is the potential (Φ). The reordered system then looks like

$$\begin{bmatrix} \boldsymbol{H}_{c,c} & -\boldsymbol{G}_{a,c} & 0 & 0 & -4\pi \\ \boldsymbol{H}_{c,a} & -\boldsymbol{G}_{a,a} & 0 & 0 & -4\pi \\ 0 & 0 & \boldsymbol{K}_c & 0 & 0 \\ 0 & -\hat{\boldsymbol{F}}_a & 0 & \boldsymbol{K}_a & 0 \\ 0 & -A_a & 0 & 0 & 0 \end{bmatrix} \begin{bmatrix} \Phi_c \\ \vec{n}\cdot\nabla\Phi_a \\ V_c \\ V_a \\ \Phi_\infty \end{bmatrix}$$

$$= \begin{bmatrix} \boldsymbol{G}_{c,c} & -\boldsymbol{H}_{a,c} \\ \boldsymbol{G}_{c,a} & -\boldsymbol{H}_{a,a} \\ \hat{\boldsymbol{F}}_c & 0 \\ 0 & 0 \\ A_c & 0 \end{bmatrix} \begin{bmatrix} \vec{n}\cdot\nabla\Phi_c \\ \Phi_a \end{bmatrix} \tag{63}$$

where the column matrix on the left hand side is the set of unknown variables and the column matrix on the right side is the set of known boundary conditions. Equation (63) can be rewritten as

$$[\boldsymbol{A}] \begin{bmatrix} \Phi_c \\ \vec{n}\cdot\nabla\Phi_a \\ V_c \\ V_a \\ \Phi_\infty \end{bmatrix} = [\boldsymbol{B}] \begin{bmatrix} \vec{n}\cdot\nabla\Phi_c \\ \Phi_a \end{bmatrix} \tag{64}$$

where $\boldsymbol{A}$ and $\boldsymbol{B}$ correspond to the matrices in eqn (63).

If the boundary conditions are constant, the unknown variables can be obtained by a simple matrix inversion. For problems in electrochemistry, the set of known boundary conditions are given as a set of nonlinear functions of the unknown variables. Therefore, the solution must be obtained using a technique for coupled sets of nonlinear algebraic equations. This is done by rewriting eqn (64) as a function that is equal to zero

$$[\boldsymbol{A}] \begin{bmatrix} \Phi_c \\ \vec{n}\cdot\nabla\Phi_a \\ V_c \\ V_a \\ \Phi_\infty \end{bmatrix} - [\boldsymbol{B}] \begin{bmatrix} \vec{n}\cdot\nabla\Phi_c = f(V,\Phi_c) \\ \Phi_a = f(V,\vec{n}\cdot\nabla\Phi_a) \end{bmatrix} = \begin{bmatrix} 0 \\ 0 \\ 0 \\ 0 \\ 0 \end{bmatrix}. \tag{65}$$

Since one of the column matrices contains unknown variables, a guess for the values must be made. Since the guess will not be the correct solution to eqn (65), the right

hand column vector will not be equal to zero, but a residual

$$[\boldsymbol{A}]\begin{bmatrix} \Phi_c \\ \vec{n}\cdot\nabla\Phi_a \\ V_c \\ V_a \\ \Phi_\infty \end{bmatrix} - [\boldsymbol{B}]\begin{bmatrix} f(V,\Phi_c) \\ f(V,\vec{n}\cdot\nabla\Phi_a) \end{bmatrix} = \begin{bmatrix} R \end{bmatrix}. \tag{66}$$

Rewriting eqn (65) as a general set of equations of an unknown vector $\boldsymbol{x}$

$$\boldsymbol{F}(\boldsymbol{x}) = \boldsymbol{0} \tag{67}$$

a Jacobian $\boldsymbol{J}$, of the set of equations can be written where an element in the Jacobian is given by

$$\boldsymbol{J}_{i,j} = \left.\frac{\partial \boldsymbol{F}_i}{\partial \boldsymbol{x}_j}\right|_{\boldsymbol{x}_{\ell\neq j}}. \tag{68}$$

Then the Newton–Raphson iteration can be performed to obtain the solution vector $\boldsymbol{x}$ such that eqn (67) holds. Again the line search is necessary for the the method to work. However, in most non-trivial cases, even the line searches fail.

In order to get the method to converge to a solution, many techniques were tried including the minimal residual techniques such as the modified Powell method [50], Levenberg–Marquort techniques and other methods such as the conjugate gradient method. These techniques would converge sometimes if the guess was nearly the correct value. However, in general, the convergence behavior was very poor.

4.2 Variable transformation to stabilize convergence

The system of equation that result from Φ, V, i as the set of variables for the solution has very poor convergence characteristics. Great effort was required to bring the system to convergence. Standard line searches and even minimal residual techniques failed to converge.

A simple variable transformation was developed that enables good convergence properties using the simple line search method. The variable transformation needed can be readily identified from the equations such as (9) used to describe the reaction kinetics. In eqn (9), the difference $V - \Phi$ appears many times. A simple transformation can be written

$$\Psi = V - \Phi \tag{69}$$

where Ψ represents the driving force for the electrochemical kinetics. The variable V is then chosen as the dependent variable and rewritten as

$$V = \Psi + \Phi. \tag{70}$$

All of the equations used for the kinetics, $i.e.$ eqn (9) for bare metal, eqn (12) for coated metal, eqn (13) for galvanic anodes, and eqn (16) for impressed current

anodes, can be rewritten in terms of the new variable. For bare metal, one obtains

$$i = 10^{(\Psi - E_{\mathrm{Fe}})/\beta_{\mathrm{Fe}}} - \left(\frac{1}{i_{\mathrm{lim,O_2}}} + 10^{(\Psi - E_{\mathrm{O_2}})/\beta_{\mathrm{O_2}}} \right)^{-1} - 10^{-(\Psi - E_{\mathrm{H_2}})/\beta_{\mathrm{H_2}}} \quad (71)$$

For coated metal, two simultaneous equations in two unknowns describe the current density, $i.e.$

$$i = \frac{-(\Phi - \Phi_{\mathrm{in}})}{\rho_{\mathrm{film}} \delta_{\mathrm{film}}} \quad (72)$$

and

$$\begin{aligned} i = \frac{A_{\mathrm{pore}}}{A} \Bigg[& 10^{(\Psi + \Phi - \Phi_{\mathrm{in}} - E_{\mathrm{Fe}})/\beta_{Fe}} \\ & - \left(\frac{1}{(1 - \alpha_{\mathrm{blk}}) i_{\mathrm{lim,O_2}}} - 10^{(\Psi + \Phi - \Phi_{in} - E_{\mathrm{O_2}})/\beta_{\mathrm{O_2}}} \right)^{-1} \\ & - 10^{-(\Psi + \Phi - \Phi_{\mathrm{in}} - E_{\mathrm{H_2}})/\beta_{\mathrm{H_2}}} \Bigg]. \end{aligned} \quad (73)$$

For galvanic anodes,

$$\Psi = E_{\mathrm{anode}} + \beta_{\mathrm{anode}} \log(i/i_{\mathrm{corr}} + 1) \quad (74)$$

and for impressed current anodes,

$$\Psi = \triangle V_{\mathrm{rectifier}} + E_{\mathrm{O_2}} + \beta_{\mathrm{O_2}} \log(i/i_{\mathrm{corr}} + 1) \quad (75)$$

where $\triangle V_{\mathrm{rectifier}}$ is the known setting for the rectifier.

The set of equations for the finite element method must also be rewritten as

$$\boldsymbol{K}\,[\Psi + \Phi] = [f] \quad (76)$$

where f and $\boldsymbol{K}$ do not change. The boundary element method is not changed. The set of equations that is solved becomes:

$$\begin{bmatrix} 0 & 0 & \boldsymbol{H}_{c,c} & \boldsymbol{H}_{a,c} & -4\pi \\ 0 & 0 & \boldsymbol{H}_{c,a} & \boldsymbol{H}_{a,a} & -4\pi \\ \boldsymbol{K}_c & 0 & \boldsymbol{K}_c & 0 & 0 \\ 0 & \boldsymbol{K}_a & 0 & \boldsymbol{K}_a & 0 \\ 0 & 0 & 0 & 0 & 0 \end{bmatrix} \begin{bmatrix} \Psi_c \\ \Psi_a \\ \Phi_c \\ \Phi_a \\ \Phi_\infty \end{bmatrix} = \begin{bmatrix} \boldsymbol{G}_{c,c} & \boldsymbol{G}_{a,c} \\ \boldsymbol{G}_{c,a} & \boldsymbol{G}_{a,a} \\ \hat{\boldsymbol{F}}_c & 0 \\ 0 & \hat{\boldsymbol{F}}_a \\ A_c & A_a \end{bmatrix} \begin{bmatrix} \vec{n} \cdot \nabla \Phi_c \\ \vec{n} \cdot \nabla \Phi_a \end{bmatrix}. \tag{77}$$

At this point the essential boundary condition for V $(\Psi + \Phi)$ is applied. There is one degree of freedom in the problem for this potential so one node on one pipe is selected to have a 0 potential. This is done by replacing the FEM equation for the single selected node in the system given by eqn (77) with

$$\Psi + \Phi = 0. \tag{78}$$

The FEM equation (lower half of the system) is replaced because that is where the degree of freedom in the reference potential is. If there are multiple CP systems, then there must be an equal number of essential boundary conditions on $\Psi + \Phi$. Once the equations are set up, all unknown variables are placed on the left-hand-side, which are Φ and Ψ for cathodes (pipes, tank bottoms, ship hulls, *etc*.) and $\vec{n} \cdot \nabla \Phi$ and Φ for anodes. The reordered system of equations is

$$\begin{bmatrix} 0 & -\boldsymbol{G}_{a,c} & \boldsymbol{H}_{c,c} & \boldsymbol{H}_{a,c} & -4\pi \\ 0 & -\boldsymbol{G}_{a,a} & \boldsymbol{H}_{c,a} & \boldsymbol{H}_{a,a} & -4\pi \\ \boldsymbol{K}_c & 0 & \boldsymbol{K}_c & 0 & 0 \\ 0 & -\hat{\boldsymbol{F}}_a & 0 & \boldsymbol{K}_a & 0 \\ 0 & -A_a & 0 & 0 & 0 \end{bmatrix} \begin{bmatrix} \Psi_c \\ \vec{n} \cdot \nabla \Phi_a \\ \Phi_c \\ \Phi_a \\ \Phi_\infty \end{bmatrix} = \begin{bmatrix} \boldsymbol{G}_{c,p} & 0 \\ \boldsymbol{G}_{c,a} & 0 \\ \hat{\boldsymbol{F}}_c & 0 \\ 0 & -\boldsymbol{K}_a \\ A_c & 0 \end{bmatrix} \begin{bmatrix} \vec{n} \cdot \nabla \Phi_c \\ \Psi_a \end{bmatrix}. \tag{79}$$

This system has excellent convergence characteristics and uses about the same number of iterations as a system without the effects of the pipe metal included.

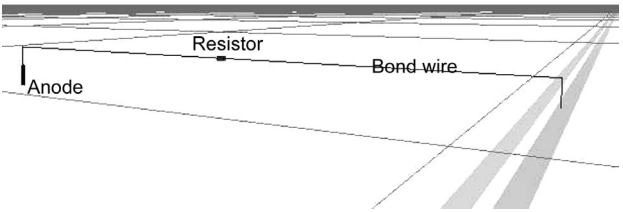

Figure 6: Portion of the configuration of 2 pipes plus 1 of the anodes providing protective current. The display includes an optional resistor in the connecting bond.

5 Examples

The above development provides a foundation for modeling cathodic protection of long stretches of multiple pipelines, including interaction among cathodic protection networks, while retaining the flexibility to account for the role of discrete coating holidays. Care must be taken in the implementation of the approach presented above. Adaptive integration techniques are needed to generate values of sufficient accuracy for the terms appearing in the coefficient matrices. An efficient nonuniform meshing algorithm is needed to avoid numerical errors associated with abrupt changes in mesh size while minimizing the computational cost of the program.

Two examples are included here to show the potential of the model described above. The first shows the calculation of multiple CP systems for two closely spaced pipes in a right-of-way with coating holidays. The second shows how the electrical midpoint may be found.

5.1 Multiple CP Systems

The following example concerns 2 pipelines in a right-of-way protected by separate cathodic protection systems. Three miles of pipe are modeled with both pipes exhibiting several coating holidays. A portion of the model is shown in fig. 6. The smaller pipe is assumed to be older and to have a poor quality coating, while the larger was assumed to have the better coating. No bonds connect the two CP systems.

When the complete system is modeled using the methods given in section 3.6, the current density integrated across the surface of each object (anode or pipe) sum to zero for each CP system, as demonstrated in table 3. As indicated in table 3, Pipe 1, Anode 1, and Anode 3 comprise CP System 1; and Pipe 2 and Anode 2 comprise CP System 2. The amount of current drawn from Anodes 1 and 3 depends on the potential applied and on the quality of the coating on adjacent portions of the pipe.

Even though the two pipelines were electrically isolated from each other, they still influenced the respective level of cathodic protection through the influence of potential gradients in the soil. A plot of current density along the length of one of the two pipes is shown in fig. 7. It is interesting to note that the pipe presented in fig. 7 does not have a holiday at position 1.61km, but the adjacent pipe does. A sharp

Table 3: Current density integrated over the surface of objects.

Object	CP System 1	CP System 2
Pipe 1	−0.40180 A	0 A
Pipe 2	0 A	−0.26287 A
Anode 1	0.35655 A	0 A
Anode 2	0 A	0.26287 A
Anode 3	0.04525 A	0 A
Total	0 A	0 A

decrease in the cathodic current (seen as a spike due to the scale used) appears on the pipe due to the large current demand associated with the coating defect on the adjacent pipe. The same area is shown in a false color plot in fig. 8. A shadow effect is seen on both objects due to the larger current density drawn to the coating defect as compared to that required by the coated regions.

The solution to the potential distribution within the pipe steel allows investigation of the flow of current back to the anodes. The current vectors in the pipe steel in the vicinity of a large coating holiday are presented in fig. 9. The dark rectangle represents a large coating defect which exposes bare steel. The surrounding area is covered by intact coating. The vectors drawn show how the current entering the pipe metal through the holiday spreads within the pipe steel.

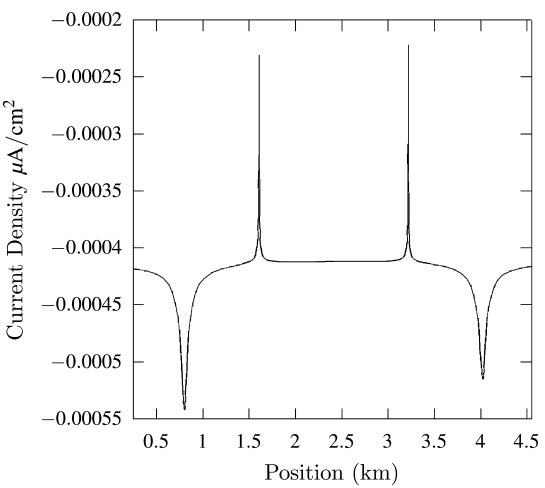

Figure 7: Calculated current density as a function of axial position for Pipe 1. The current density was obtained for the section of pipe directly facing the other pipe.

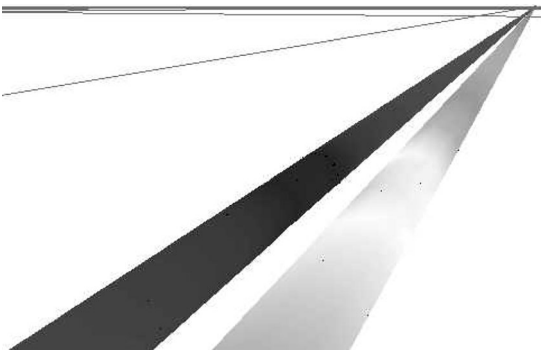

Figure 8: False color image of current density. The lighter color indicates lower current density.

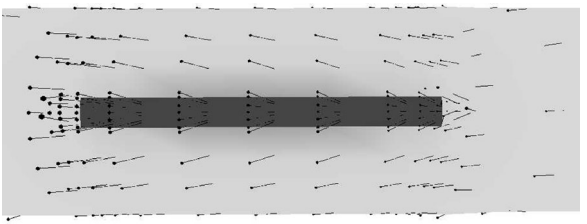

Figure 9: False color image of current flow through the pipe metal. The flow vectors indicate that the current entering the pipe metal through the holiday spreads within the pipe steel.

5.2 Electrical midpoint

Electrical midpoints can also be determined from the steel voltage solution. To demonstrate, a 4-mile long pipeline is modeled with three anodes placed along its

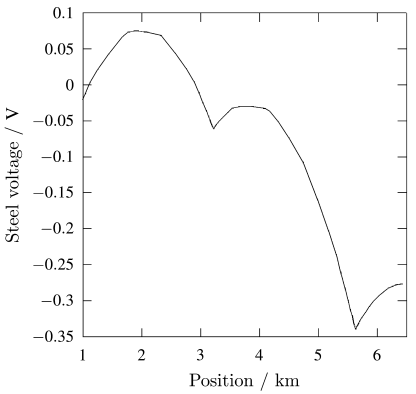

Figure 10: Potential in the steel as a function of axial position. The electrical midpoint can be identified by the maxima between cusps associated with connections to the anodes.

length. The anodes are set to different driving potentials. The potential in the steel, referenced to the potential at the start of the pipe, is presented in fig. 10.

The reference location is given by the node for which eqn (78) applies. The sharp minima or cusps shown in fig. 10 are associated with connections to anodes, ground beds, or other pipes. The electrical midpoints can be identified by the maxima between cusps. As seen in fig. 10, there are two maxima along the length which indicate the locations of the electrical midpoints.

6 Conclusions

This chapter shows how a rigorous first-principles-based model for cathodic protection of multiple pipelines in a right-of-way with coating holidays can be developed which accounts for all effects associated with the interaction of the pipes, anodes and other parts of the CP system. Large shadow effects are seen when coating holidays are included or when two pipes have different coating qualities.

It should be noted the cathodic protection model requires locally valid polarization curves which describe the chemistry at the pipe–soil interface. The polarization curves account for the local soil conditions such as chemistry, coating condition, and anode performance.

Acknowledgements

This work was supported by the Pipeline Research Council International and by the Gas Research Institute under Contract PR-101-9512.

References

[1] Gas facts: Distribution and transmission miles of pipeline. Technical report, American Gas Association, 1999. www.aga.org/StatsStudies/GasFacts/2131.html.

[2] Pipline accident summary report: Pipeline rupture, liquid butane release, and fire, Lively, Texas August 24, 1996. Technical report, National Transportation Safety Board, Washington, D.C., 1998.

[3] Morgan, J., *Cathodic Protection*. NACE, International: Houston, TX, 2nd edition, 1993.

[4] Wagner, J., *Cathodic Protection Design I*. NACE, International, Houston, TX, 1994.

[5] Peabody, A.W., *Control of Pipeline Corrosion*. NACE: Houston, TX, 1978.

[6] Newman, J.S., *Electrochemical Engineering*. Prentice-Hall: Englewood Cliffs, New Jersey, 2nd edition, 1991.

[7] Orazem, M.E., Esteban, J.M., Kenelley, K.J. & Degerstedt, R.M., Mathematical models for cathodic protection of an underground pipeline with coating holidays: Part 1. theoretical development. *Corrosion*, **53(4)**, pp. 264–272, 1997.

[8] Yan, J.F., Pakalapati, S.N.R., Nguyen, T.V., White, R.E. & Griffin, R.B., Mathematical modeling of cathodic protection using the boundary element method with a nonlinear polarization curve. *Journal of the Electrochemical Society*, **139(7)**, pp. 1932–1936, 1992.

[9] Kennelley, K.J., Bone, L. & Orazem, M.E., Current and potential distribution on a coated pipeline with holidays: Part 1. model and experimental verification. *Corrosion*, **49(3)**, pp. 199–210, 1993.

[10] Nisançiöglu, K., Predicting the time dependence of polarization on cathodically protected steel in seawater. *Corrosion*, **43**, pp. 100–111, 1987.

[11] Nisançiöglu, K., Gartland, P.O., Dahl, T. & Sander, E., Role of surface structure and flow rate on the polarization of cathodically protected steel in seawater. *Corrosion*, **43**, pp. 710–718, 1987.

[12] Nisançiöglu, K. & Gartland, P.O., Current distribution with dynamic boundary conditions. *I. Chem. Symposium Series No. 112: Conference on Electrochemical Engineering*, Loughborough University of Technology: Loughborough, 1989.

[13] Carson, S.L. & Orazem, M.E., Time-dependent polarization of behavior of pipeline-grade in low ionic strength environments. *Journal of Applied Electrochemistry*, **29**, pp. 703–717, 1999.

[14] Anderko, A. & Young, R.D., Model for corrosion of carbon steel in lithium bromide absorption refrigeration systems. *Corrosion*, **56(5)**, pp. 543–555, 2000.

[15] Anderko, A., MacKenzie, P. & Young, R.D., Computation of rates of general corrosion using electrochemical and thermodynamic models. *Corrosion*, **57(3)**, pp. 202–213, 2001.

[16] Korzhenko, A., Tabellout, M. & Emery, J., Dielectric relaxation properties of the polymer coating during its exposition to water. *Materials Chemistry and Physics*, **65(3)**, pp. 253–260, 2000.

[17] Corfias, C., Pebere, N. & Lacabanne, C., Characterization of a thin protective coating on galvanized steel by electrochemical impedance spectroscopy and a thermostimulated current method. *Corrosion Science*, **41(8)**, pp. 1539–1555, 1999.

[18] Margarit, I. & Mattos, O., About coatings and cathodic protection: Possibilities of impedance as monitoring technique. *Electrochemical Methods in Corrosion Research VI, Parts 1 and 2*, Transtec Publications: Zurich-Eutikon, pp. 279–292, 1998.

[19] Thompson, I. & Campbell, D., Interpreting nyquist responses from defective coatings on steel substrates. *Corrosion Science*, **36(1)**, pp. 187–198, 1994.

[20] Bellucci, F. & Nicodemo, L., Water transport in organic coatings. *Corrosion*, **49(3)**, pp. 235–247, 1993.

[21] Diakow, D., Van Boven, G. & Wilmott, M., Polarization under disbonded coatings: Conventional and pulsed cathodic protection compared. *Materials Performance*, **37(5)**, pp. 17–23, 1998.

[22] Jack, T.R., External corrosion of line pipe: a summary of research activities. *Materials Performance*, **35(3)**, pp. 18–24, 1996.

[23] Beavers, J.A. & Thompson, N.G., Corrosion beneath disbonded pipeline. *Materials Performance*, **36(4)**, pp. 13–19, 1997.

[24] Riemer, D. & Orazem, M., Development of mathematical models for cathodic protection of multiple pipelines in a right of way. *Proceedings of the 1998 International Gas Research Conference*, Gas Research Institute, GRI: Chicago, p. 117, 1998. Paper TSO-19.

[25] Riemer, D.P. & Orazem, M.E., Cathodic protection of multiple pipelines with coating holidays. *Proceedings of the NACE99 Topical Research Symposium: Cathodic Protection: Modeling and Experiment*, ed. M.E. Orazem, NACE, NACE International: Houston, TX, pp. 65–81, 1999.

[26] Jones, D.A., *Principles and Prevention of Corrosion*. Prentice Hall: Upper Saddle River, NJ, 1996.

[27] Carslaw, H.S. & Jaeger, J.C., *Conduction of Heat in Solids*. Oxford University Press: New York, 1959.

[28] Moulton, H.F., Current flow in rectangular conductors. *Proceedings of the London Mathematical Society*, **ser. 2(3)**, pp. 104–110, 1905.

[29] Bowman, F., *Introduction to Elliptic Functions with Applications*. John Wiley and Sons: New York, 1953.

[30] Orazem, M.E. & Newman, J., Primary current distribution and resistance of a slotted-electrode cell. *Journal of the Electrochemical Society*, **131(12)**, pp. 2857–2861, 1984.

[31] Orazem, M.E., Calculation of the electrical resistance of a compact tension specimen for crack-propagation measurements. *Journal of the Electrochemi cal Society*, **132(9)**, pp. 2071–2076, 1985.

[32] Orazem, M.E. & Ruch, W., An improved analysis of the potential drop method for measuring crack lengths in compact tension specimens. *International Jour nal of Fracture*, **31**, pp. 245–258, 1986.

[33] Diem, C.B., Newman, B. & Orazem, M.E., The influence of small machining errors on the primary current distribution at a recessed electrode. *Journal of the Electrochemical Society*, **135**, pp. 2524–2530, 1988.

[34] Brebbia, C.A. & Dominguez, J., Boundary element methods for potential problems. *Applied Mathematical Modelling*, **1(7)**, pp. 371–378, 1977.

[35] Aoki, S., Kishimoto, K. & Sakata, M., Boundary element analysis of galvanic corrosion. *Boundary Elements VII*, eds. C.A. Brebbia & G. Maier, Springer-Verlag: Heidelberg, volume 1, pp. 73–83, 1985.

[36] Telles, J., Wrobel, L., Mansur, W. & Azevedo, J., Boundary elements for cathodic protection problems. *Boundary Elements VII*, eds. C.A. Brebbia & G. Maier, Springer-Verlag, volume 1, pp. 63–71, 1985.

[37] Zamani, N. & Chuang, J., Optimal-control of current in a cathodic protection system: a numerical investigation. *Optimal Control Applications & Methods*, **8(4)**, pp. 339–350, 1987.

[38] Brichau, F. & Deconinck, J., Numerical model for cathodic protection of buried pipes. *Corrosion*, **50(1)**, pp. 39–49, 1994.

[39] Brichau, F., Deconinck, J. & Driesens, T., Modeling of underground cathodic protection stray currents. *Corrosion*, **52**, pp. 480–488, 1996.

[40] Aoki, S. & Amaya, K., Optimization of cathodic protection system by BEM. *Engineering Analysis with Boundary Elements*, **19(2)**, pp. 147–156, 1997.
[41] Aoki, S., Amaya, K. & Miyasaka, M., Boundary element analysis of cathodic protection for complicated structures. *Proceedings of the NACE99 Topical Research Symposium: Cathodic Protection, Modeling and Experiment*, ed. M.E. Orazem, NACE, NACE International: Houston, TX, pp. 45–65, 1999.
[42] Brebbia, C. & Dominguez, J., *Boundary Elements: An Introductory Course*. McGraw-Hill, The Bath Press: Avon, Great Britain, 1989.
[43] Brebbia, C.A., Telles, J.C.F. & Wrobel, L.C., *Boundary Element Techniques*. Springer-Verlag: Heidelberg, 1984.
[44] Hartmann, F., Katz, C. & Protopsaltis, B., Boundary elements and symmetry. *Ingenieur Archiv*, **55(6)**, pp. 440–449, 1985.
[45] Gray, L. & Paulino, G., Symmetric Galerkin boundary integral formulation for interface and multi-zone problems. *International Journal for Numerical Methods in Engineering*, **40**, pp. 3085–3101, 1997.
[46] Stakgold, I., *Green's Functions and Boundary Value Problems*. John Wiley & Sons: New York, 1979.
[47] Dwight, H.B., Calculations of resistance to ground. *Electrical Engineering*, **55**, p. 1319, 1936.
[48] Telles, J.C.F. & Paula, F.A.D., Boundary elements with equilibrium satisfaction: A consistent formulation for potential and elastostatic analysis. *International Journal of Numerical Methods in Engineering*, **32**, pp. 609–621, 1991.
[49] Trevelyan, J. & Hack, H., Analysis of stray current corrosion problems using the boundary element method. *Boundary Element Technology IX*, Computational Mechanics Publications: Boston, pp. 347–356, 1994.
[50] Burton, S., Garbow, K.E., Hillstrom, J.J. & Others, Modified powell method with analytic jacobian. Software source code hybrdj.f, 1980. Argonne National Laboratory. minpack project. www.netlib.org/minpack.